Fluid-enhanced neotectonic faulting in the cratonic lithosphere of the Nullarbor Plain, Australia

H. Yang[1, 2], S. Sellmann[1], M. Quigley[1]

Affiliation 1: School of Earth Sciences, University of Melbourne, Victoria

Affiliation 2: Research School of Earth Sciences, Australian National University, Canberra

Corresponding author: Haibin Yang (haibin.yang@anu.edu.au)

Key Points:

- The Nullarbor plain in Australia is a stable craton but characterized by active fault (fold) traces of 7-150 km long.
- The displacement is not positively related to fault length but is spatially linked to high electrical conductors in the lithosphere.
- Lithospheric fluid localization may have weakened pre-existing faults and enhanced neotectonic faulting in the Nullarbor plain.

Abstract

The Nullarbor Plain is underlain by a thick cratonic lithospheric mantle, which is thought to have a paucity of neotectonic faults and seismicity. Based on the analysis of high-resolution digital elevation models, identified neotectonic fault traces on the nearly flat karst landscape locally extend >100 km long, suggesting potential for hosting large (>7.3 to 7.5) moment magnitude earthquakes. The measured cumulative along-strike maximum displacement D_{max} for each trace is not proportional to surface rupture length (L) but is correlated with the occurrence of crust-scale electrical conductors identified in magnetotelluric surveys. Two major conductors penetrate from the upper crust to the topmost mantle along crustal scale shear zones. The conductivity value in the topmost mantle is much higher than in the cratonic mantle, indicating serpentinization of the mantle with the addition of fluids. Lithospheric fluid localization may have weakened pre-existing faults and enhanced neotectonic faulting in the Nullarbor plain.

Plain Language Summary

Stable continental cratons on the Earth are generally thought to be immune from large earthquakes. The paucity of historic earthquakes on many intraplate faults can give residents a false sense of seismic security, even though intraplate earthquakes have caused more fatalities than interplate earthquakes. The long recurrence time makes it difficult for paleo-earthquake studies because the surface erosional processes could have removed all the scarps of historic earthquake ruptures. Finding an ideal place that can provide sufficient observations of

intracontinental active faults is challenging but pivotal for unravelling intracontinental fault dynamics and seismic hazard assessment. The nearly flat Nullarbor Plain in South-Central Australia is covered by 100s-meter-thick limestone, which is cut by reactivated reverse faults inherited from Precambrian bedrock structures. The limestone has been exposed to the surface since mid-Miocene. The arid climate in this region has helped preserve these neotectonic features from surface erosion. The fault traces with high displacements can be well correlated with the patches with high electrical conductivities, which is sensitive to fluids in the lithosphere. With co-located seismic reflections profiles, gravity, and magnetic maps, we propose that the enhanced neotectonic activities are likely to be caused by fluids from deep part of the lithosphere.

Introduction

The high integrated brittle strength of cratons with a cool and thick lithosphere protects cratonic interiors from tectonic deformation. The paucity of neotectonic (i.e., 0-10 Ma) faults and seismicity in cratons relative to peripheral intraplate geological domains (e.g., fossil continental rift zones) and plate boundaries provides evidence for enhanced lithospheric strength and its role in limiting tectonic deformation. Tectonism is typically concentrated in places with relatively low integrated brittle strength Lenardic et al., 2003Naliboff and Buiter, 2015Yang et al., 2018(; ;), e.g., plate boundaries. High strain rates ($>10^{-15}$ s^{-1}) at plate boundaries facilitate enhanced faulting. Energy radiated by interplate seismogenic faulting events accounts for >99% global seismic moment release Johnston, 1989Kagan, 1997(;). In contrast, stable cratons with lower strain rates ($<\sim10^{-16}$ s^{-1}) are mostly quiescent of large earthquakes and faulting Fagereng and Biggs, 2019(). Seismic quiescence may in some cases relate to short instrumental histories (< ~150 years) with respect to the earthquake cycles ($>10^4$ years) and the limited resolution of geodetic surveys for fault motions in stable cratons Leonard et al., 2014(). However, neotectonic faulting and historical surface-rupturing earthquakes have occurred throughout Australia's cratons Clark et al., 2012King et al., 2019Quigley et al., 2010Yang et al., 2021(; ; ;). Repeated surface-rupturing earthquakes on a single fault may enable fault lengthening through lateral propagation and linkage Cowie and Scholz, 1992b() and can accumulate displacements that can be quantified through analyses of neotectonic features, e.g. faults or fault-related folds. The flat Nullarbor Plain is suggested to have low surface erosion rates, as indicated from preservation of shallow caves dissolved in the early Pliocene and erosionally-etched low amplitude surface undulations (1-2 meter in a wavelength of 300-900m) of Pliocene-Pleistocene dune relicts Burnett et al., 2020Miller et al., 2012(;). The slow rates of erosion and flatness of cratons also provide excellent fault scarp preservation and present opportunities to examine fault evolution over Myr timescales.

The Proterozoic basement underneath the nearly featureless Nullarbor Plain, composed of the Madura province (west) and Coompana province (east) (Fig.1-

3), demonstrates lower teleseismic P wave attenuation and seismic activity than the Yilgarn craton to the west Bezada and Smale, 2019(). The magnetotelluric survey shows that high electrical resistivity ($>10^4$ Ω m) in the mantle underneath the Nullarbor Plain extends to 200 km depth Wise and Thiel, 2019(), indicating a cratonic lithosphere like the neighboring Gawler craton to the East Artemieva and Mooney, 2001().

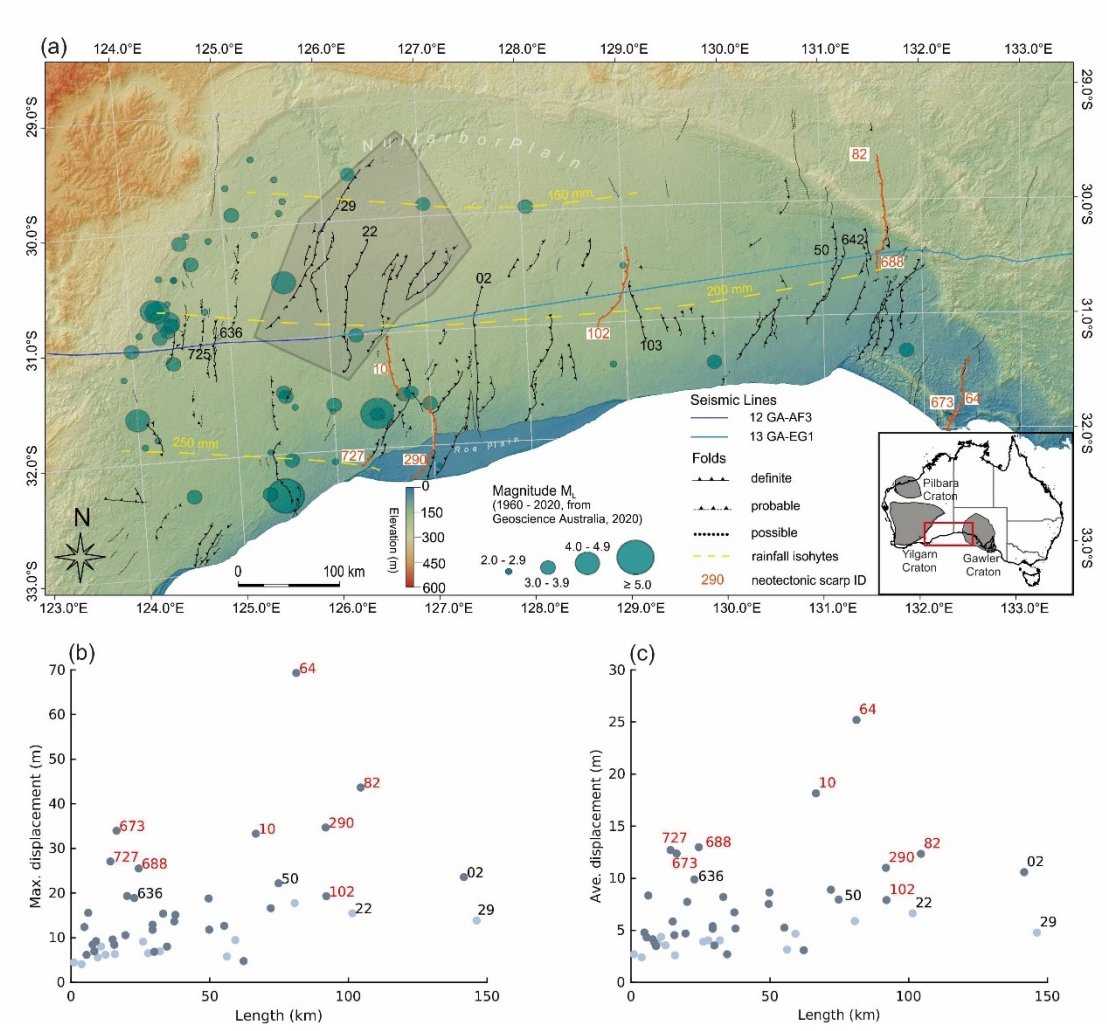

Figure 1. (a) Topographic map of the Nullarbor Plain, Australia. Black (or red) lines mark the neotectonic fold (or fault) traces on the surface. The circles are regional earthquakes (1970-2020) from the Geoscience Australia catalog. The traces in the northwestern part are demarcated by a shaded polygon, which is referred to as the interior region in this study. The dashed yellow contours represent

annual precipitations. The inset map illustrates tectonic settings of the study area, which is located between the Archean Yilgarn and Gawler craton. Displacement for each trace is measured. The maximum and average displacement versus fault length is shown in (b) and (c), respectively. The light grey dots represent data from the Northwestern part, shaded polygon in (a). Some of these traces that have a relatively high displacement or length are labeled with the number of each trace, which is shown in (a) adjacent to each fault trace. The label colors in (b) and (c) are also consistent with the fault color in (a). The red one generally has high displacements.

The 200,000 km^2 surface of the Nullarbor Plain is covered by 100s-meter-thick limestones Scheib et al., 2016(), which are cut by reactivated reverse faults inherited from bedrock structures Clark et al., 2012(). The limestone has been exposed at the surface since mid-Miocene Hou et al., 2008Lowry and Jennings, 1974(;). Reverse faulting in southern Australia is attributed to approximately E-W oriented most compressive stress (SH_{max}) originating from plate boundary forces that have increased since 10-5 Ma Coblentz et al., 1995Quigley et al., 2010Sandiford et al., 2004(; ;). The Miocene age of the faulted limestones and late Miocene onset of neotectonic faulting elsewhere provides the oldest age limit for inception of neotectonic faulting on the Nullarbor Plain. The arid climate in this region has helped preserve these neotectonic features from surface erosions Sandiford and Quigley, 2009(). Previous paleo-earthquake studies in the Nullarbor Plain have revealed that some neotectonic traces are >100 km long Clark et al., 2012(). Rupturing along the entire length would produce an earthquake of M_w 7.3 to 7.5, according to the empirical relationships between rupture length and M_w Wells and Coppersmith, 1994Yang et al., 2021(;). What controls the spatial distribution and prehistoric activity of these neotectonic traces on the Nullarbor Plain is not well understood.

Digital elevation models (DEMs) have been recently used to map linear features on the surface and identify those of neotectonic faulting origin. The vertical offset along each trace has been measured to establish a detailed along-strike displacement profile (see Methods in Supplementary Material). The mapped neotectonic traces are commonly aligned with magnetic lineaments and normal to maximum gravity gradient direction. The 12GA-AF3 and 13GA-EG1 seismic reflection profiles across the Nullarbor Plain (Fig. 2) Costelloe et al., 2012Holzschuh, 2015(;), which intersect many of the observed neotectonic traces, are used to constrain the crust-scale fault geometries and physical properties. The regional magnetotelluric profiles (Fig. 3) are utilized to analyze the electrical conductivities that are sensitive to fluids in the lithosphere Constable, 1993(), which can significantly reduce the rheological strength of a fault for both the brittle and ductile deformation Brace and Kohlstedt, 1980Karato and Jung, 1998(;).

Neotectonic features

The mapped neotectonic traces demonstrate a north- to northeast- trending orientation (Fig. 1-3) that is nearly normal to the east-west oriented, regional horizontal

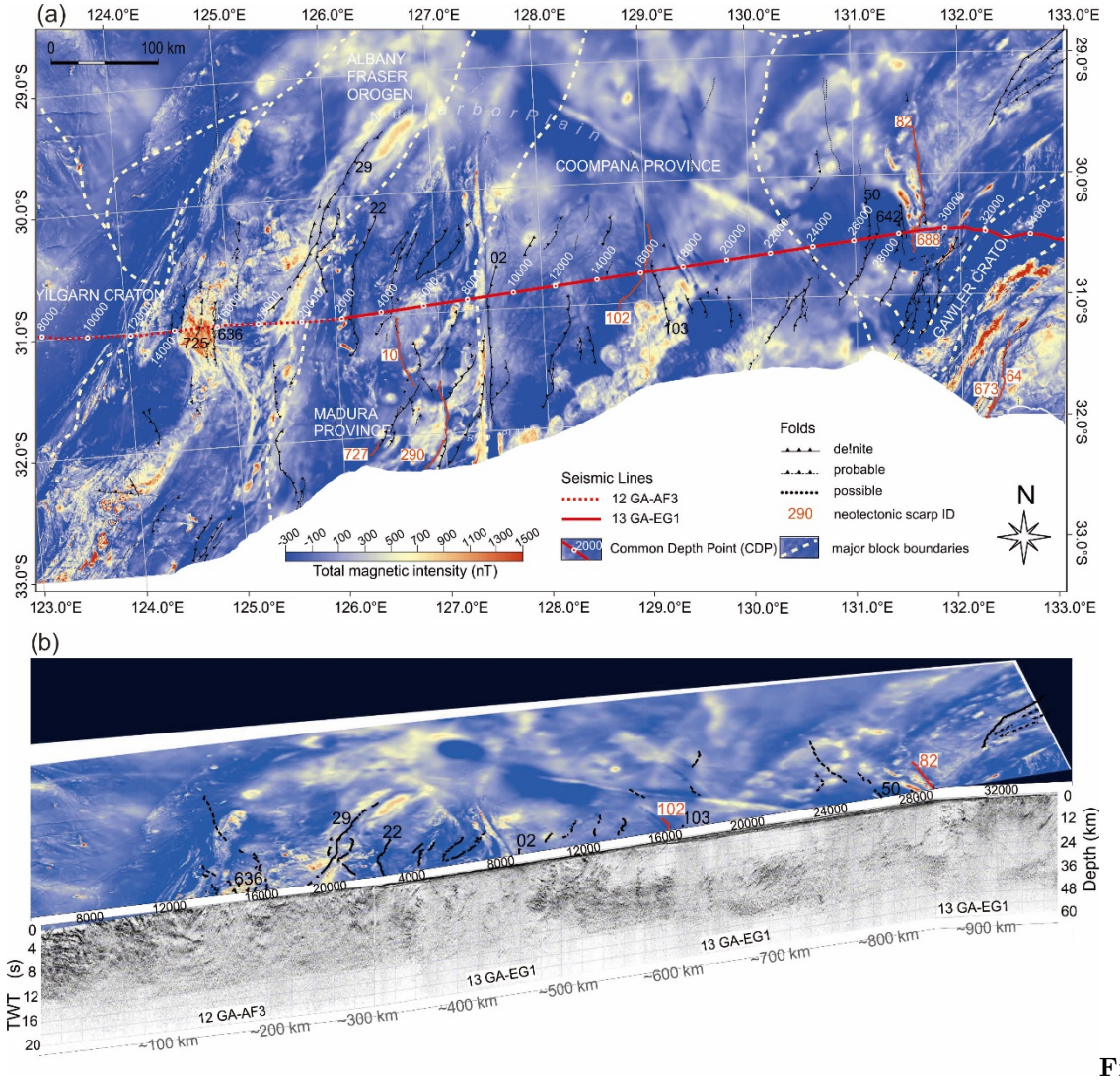

Figure 2. (a) Tectonic settings in the Nullarbor plain shown on the total magnetic intensity map (https://portal.ga.gov.au/persona/gads)**. (b) Migrated seismic reflection profiles, 12GA-AF3 and 13GA-EG1, crossing the Nullarbor Plain. The vertical axis of the seismic profile is the two-way time (TWT, 0-20 s), and the time-to-depth conversion is calculated with the velocity of 6 km s^{-1}.**

maximum compressive stress Rajabi et al., 2017(). This implies the neotectonic scarps are consistent with reverse faulting kinematics. The length of the trace ranges from 2 km to 150 km. The net displacement is calculated based on measured vertical offsets in the DEM map and fault dip angles inferred from regional seismic reflection profiles (see Methods in Supplementary Material). The 13GA-EG1 line crosses most of the eastern part of the Nullarbor Plain and cuts many measured fault/fold traces Holzschuh, 2015(), and the 12GA-AF3 line covers the western half of the study area Costelloe et al., 2012().

To investigate how the accumulated faulting-induced ground surface displacement varies with the fault length in the Nullarbor Plain, we plot the maximum surface displacement D_{max} versus the mapped surface rupture length (L) in Fig. 1b. The dataset exhibits large scatter and there is no clear positive relationship between D_{max} and L, distinct from the expected linear displacement-length relationship observed from progressive deformation accumulation in fault growth models Cowie and Scholz, 1992a(). Fold traces f02 or f29, which extend more than 140 km, show $D_{max} < 30$ m. In contrast, the fold traces f290 or f102, which are less than 100 km long, show $D_{max} > 30$ m. Further analyzing the spatial distribution of D_{max}, we find that those located in the northwest interior of the Nullarbor Plain have a relatively small D_{max} (light grey dots in Fig. 1b), and those close to the current coastline to the southern and the eastern boundary have relatively high values. Apart from the study on the relationship between slip maxima and length, the average slip shows the same result (Fig. 1c).

If these faults are assumed to be reactivated at the same time, then the ones with higher displacement should be more active (i.e., have faster slip rates and shorter inter-seismic intervals) relative to relative to equivalent-length faults with smaller displacements. The linear fault growth model Cowie and Scholz, 1992a() predicts that faults grow by tip propagation and continue to accrue displacement. This may have been the initial case for many of the Nullarbor faults and could still be the case for a subset of the faults. Fault growth via segment linkage is also likely Mansfield and Cartwright, 2001(). However, the lack of universal contemporary relationship between length and accumulated displacement suggest some faults in this dataset are likely to have increased to a critical length, perhaps controlled by the architecture of basement faults, followed by a transition to rupture behavior following the constant-length model Walsh et al., 2002(), where the fault continues to accrue displacement without increasing fault length (i.e., the rupture tips remain stationary in space through multiple

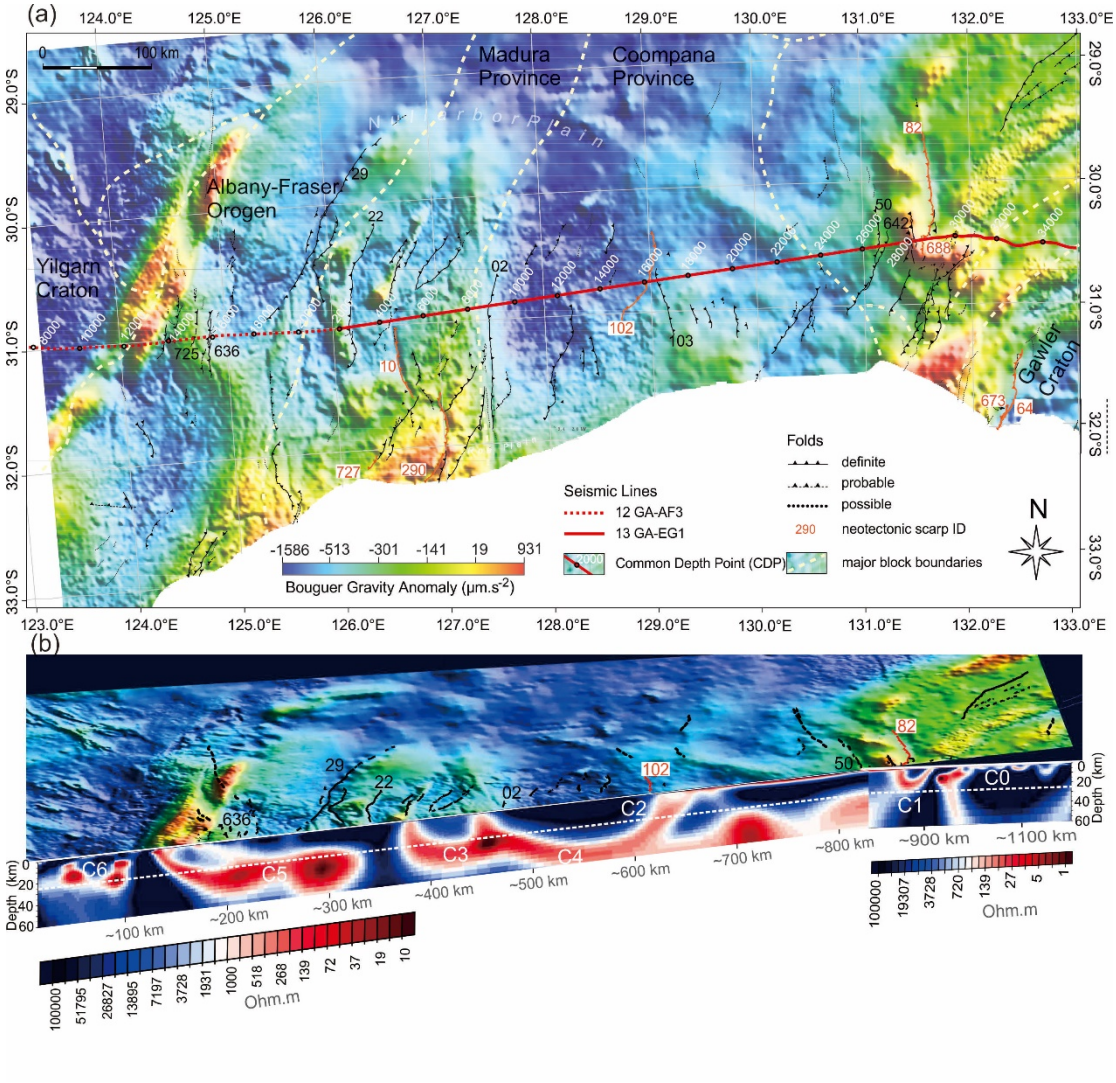

Figure 3. (a) Tectonic settings in the Nullarbor plain shown on the Bouguer Gravity anomaly map (https://portal.ga.gov.au/persona/gads)**. (b) MT profiles co-located with the 12GA-AF3 and 13GA-EG1 seismic reflection profiles crossing the Nullarbor plain. The MT profile is divided into two parts, due to the NNE striking structures to the east and the predominant N-S oriented strike to the west. The white dashed line is at the depth of 25 km, which is used to delimit the lower boundary for most of the upper crustal conductors and the upper boundary for the lower crustal conductors.**

earthquake cycles). In this case, variations in rheological strengths amongst the faults may influence their relative activity rates. As the fault *in-situ* strength

is not directly measurable, the geophysical observations can provide indirect estimation of the spatial variation of the frictional strength in the brittle upper crust and the viscous strength in the ductile lower crust Ellis et al., 2017().

Magnetotelluric profiles

The high-resolution (station spacing between 1 km and 5km) broadband (0.001-1000 s) magnetotelluric (MT) profiles (Fig. 3b) co-located with the 12GA-AF3 and 13GA-EG1 seismic reflection lines (Fig. 2b) provide a high-quality dataset to image the lithosphere conductivity properties Costelloe et al., 2012Holzschuh, 2015Wise and Thiel, 2019(; ;), which are sensitive to active or fossil fluids in the lithosphere and the related mineral precipitations, e.g., graphite and sulfides Glover, 1996(). The dimensionality analysis of the MT data for 2D inversions requires the separation of the >800-km-long profile into two parts, due to the NNE striking structures to the east (Fig. 2a and 3a) and the predominant N-S oriented strike to the west (Fig. 2a and 3a). Another earlier 450-km-long MT profile Thiel and Heinson, 2010(), with an average station distance of 18 km, located at the southeastern edge of the Nullarbor Plain, is also used to test our hypothesis. This is referred to as *Thiel2010* profile later in this paper.

Most of the neotectonic surface traces that cross the seismic reflection profiles can be well linked to subsurface reflectors (Fig. 2b and 4). With the interpreted active faults in the seismic reflection profile, the co-located MT profile is overlapped on the seismic profile to further constrain the subsurface geophysical structures related to those active faults (Fig. 4).

A spatial correlation between the high conductors in the crust and mapped surface faults with high D_{max} is revealed in Fig. 4. For the eastern part, the right lobe of conductor C1 overlaps with the fault f82 and the left lobe is related to the fault f688. For the western part, the fault f102 cuts the MT profile, but the interpreted subsurface structure is not directly located in the center of conductor C2. The fault f102 is located in an area of a resistivity of ~10^3 Ω m, but close to the conductor C2 to the East. We note that this is only a 2D profile, the northern section of the NNE oriented fault f102 might be better correlated with the conductor C2 than the southern end of f102 (Fig. 1 & 4). The left branch of the conductor C3 is located close to the fault f10. Although the

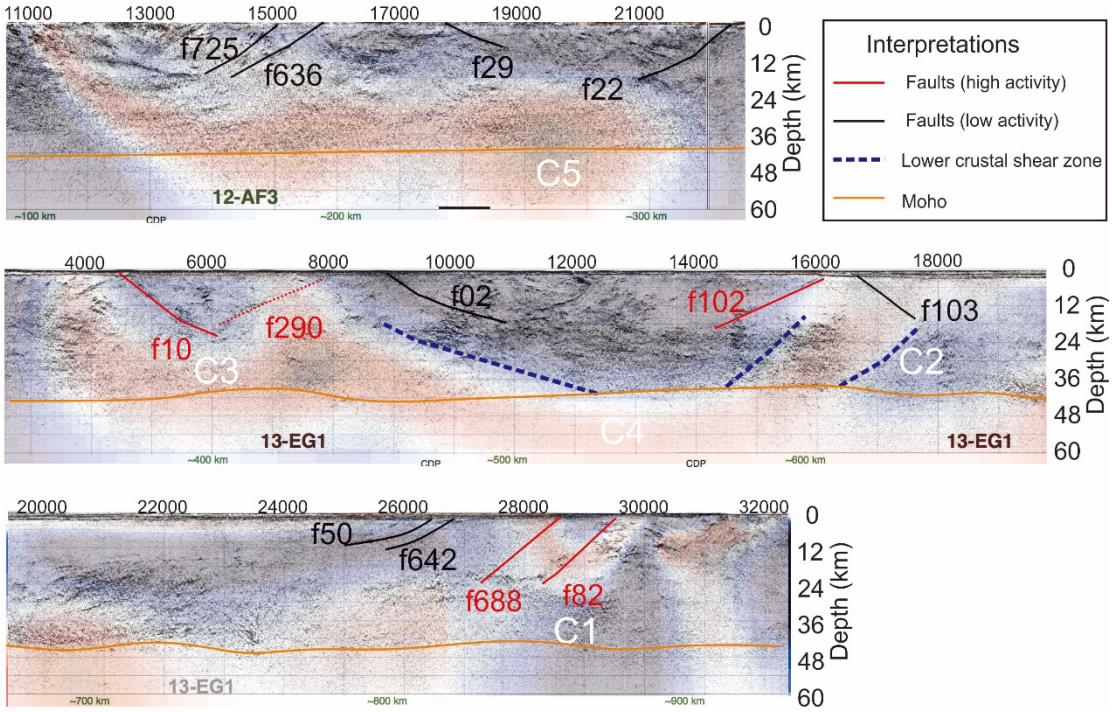

Figure 4. Interpretation of the overlapped seismic and MT profiles. For the surface-mapped faults that have corresponding reflectors on the seismic profile, those with a relatively high D_{max} and adjacent to the electrical conductors are coded with red color, otherwise, they are illustrated by black lines. The fault f290 is not directly cut by the profile, but assumed to be if northward extended, so it is marked with red dashed line. Red color in the MT profile denotes high conductivity and blue low conductivity.

right lobe of the conductor C3 is not directly cut by the fault f290, extending the right lobe of C3 straight to the south coastline is likely to be spatially correlated with the fault f290. The fault f64 at the southeastern edge of the Nullarbor Plain with the maximum D_{max} among all the mapped neotectonic traces is located right at the near vertical conductor in the *Thiel2010* profile (see conductor C2 in Fig. 11 of Thiel and Heinson, 2010). In contrast, the two longest faults f29 and f02 are not directly connected to the conductors in the upper crust, though the lower crust beneath f29 shows a clear high conductive channel (conductor C5) and the f02 offsets the right lobe of the conductor C3 center by ~30 km. The northwestern, interior faults (marked with the polygon in Fig. 1a) do not directly intersect any upper crustal conductors, though, the lower crust beneath has high conductivities (conductor C5).

Formation of active faults

The spatial correlation of faults with high D_{max} and crustal high conductors suggests a causal relationship may exist between them. High conductors could be saline fluids circulating in the fault zone or water-bearing conductive minerals. Free water in the fault zone increasing pore pressure can reduce the effective frictional strength Brace and Kohlstedt, 1980(). Weak, hydrous minerals in the fault gouge, like the smectite clay mineral found in the San Andreas fault with a frictional coefficient < 0.2 Lockner et al., 2011(), also reduces fault strength. The mineral water percolation in the fault zone with interconnected fractures as wide as several kilometers may be related to conductors in the upper brittle crust. The free water in the upper crust can be surface-derived meteoric fluids that circulate in the shallow crust.

If the surface fluids were the only source of water along the shear zone, how deep could they reach to affect the rheological strength in the crust? As pressure and temperature increase with depth, limited porosity and permeability and positive pressure gradient with depth in the ductile crust would inhibit the transfer of surface water to the deep crust without any other driving forces in a stable continent Connolly and Podladchikov, 2004(). Focusing on the conductors at depth <25 km in the MT profiles (white dashed line in Fig. 3b), there are many other near vertical (C6) or shallow conductors (C0) in the areas outside the Nullarbor Plain (Fig. 3b). Most of those conductors (C0) in the eastern part (Gawler craton) do not cut into depth > 10 km. Such depth may indicate limited penetration of surface-derived fluids into the crust. In the Nullarbor Plain, except the major conductors (C2 and C3) cutting to the middle-lower crust, shallow conductors (<15 km) like C0 and C6, which may indicate surface-derived fluids, are not observed. This is likely to be attributed to the reduced permeability in limestones with depth, due to clay mobility and concentrations, diagenesis and fracture sealing, macro-porosity clogging by microminerals, etc., which prevent meteoric fluids from penetrating to the deeper crust. On the other hand, if the conductors and fault activities were only controlled by surface fluids, the annual precipitation should be higher in the northeast areas, where f82 and f688 are located. However, the current annual precipitation in the northeast is estimated to be equivalent to those at the same latitude in the northwest interior (f29, Fig. 1a). The surface fluids can also be trapped in the middle crust through prograde burial of the fault zone under thick sedimentary sequences Raimondo et al., 2013(), which is not recorded in the geological evolution of the Nullarbor Plain since cratonization. The corollary of these observations is that the current surface-derived fluids are unlikely to form crust-scale conductivities in the Nullarbor Plain region.

Both the conductors C2 and C3 extend to and are connected in the lower crust, forming a ~100-km-long flat conductive layer at depths of 30-60 km (C4), most of which is in the topmost mantle. The continent root beneath the Nullarbor Plain with a resistivity $> 10^4$ Ω m extends to the depth of 200 km, suggesting a depleted and dry cratonic mantle Wise and Thiel, 2019(). However, the

lowest resistivity of the topmost mantle of the Nullarbor Plain at depth from 40-60 km is less than 200 Ω m. The conductivity of the lithospheric mantle is controlled by the conductivity of olivine (comprising 50-60% of the upper mantle), which can be significantly increased with temperature, but is slightly dependent on pressure Xu et al., 2000(). That means the topmost mantle with lower temperature should have higher resistivity than that at depth of 100-200 km. The global average electrical resistivity of the shallow mantle (< 100 km deep) at stable continents is > 1000 Ω m Artemieva, 2006(), which is about one order of magnitude higher than the corresponding part in the Nullarbor Plain. The low-resistivity anomaly in the Nullarbor Plain at the depth of the lower crust and shallow mantle might be attributed to serpentinization of the shallow mantle Becken and Ritter, 2012(). The electrical conductivity of serpentinized rocks have been reported to be three to four orders of magnitude higher than the un-serpentinized rocks of similar compositions, and the variation of serpentinite conductivity depends on the porosity and connection of those conducting mineral phases (e.g., magnetite) Stesky and Brace, 1973().

As the Nullarbor Plain has been situated within an intraplate continental region for hundreds of millions of years, how the shallow mantle could be serpentinized in such environment is an enigma. We propose that the conductor C4 could represent the relic of a subducted oceanic plate which has experienced serpentinization. The isotopic data from borehole-derived bedrocks suggest the Coompana Province crust is built on an oceanic crustal precursor which was dated to be ca. 1950 Ma Kirkland et al., 2017(). This is also supported by recent joint interpretations of orthogonal deep seismic reflection profiles and 3D magnetotelluric surveys Wise et al., 2018(), which suggested an ocean (Mirning Sea) between the Gawler craton and the Coompana Province with the Jindarnga Shear zone, corresponding to the fault f82 and f688 in this study, being the outboard extend of the transition zone. The relatively stable environment since cratonization might have helped preserve this serpentinite layer for > 1000 Myr. For the cold crust with a temperature gradient of 10 K km^{-1}, the upward migration rate of fluid in the ductile lower crust is estimated to be < 10 m Myr^{-1} Connolly and Podladchikov, 2004(). Without significant alternation from later thermal events, the serpentinite is likely to be detected at present time. The Cambrian serpentinite layer, part of which was cropped out to the surface, preserved in the Delamerian Orogen in southeast Australia has also been revealed by a magnetotelluric survey Robertson et al., 2015().

The concave up conductor C4 in the lower crust-to-uppermost mantle rising upwards at two edges is aligned with the lower crustal reflectors (thick blue dashed lines in Fig. 4), which represent low-angle detachment faults. This alignment in geometry indicates the dynamic process of co-deformation fluid migration. The fluid migration in a ductile shear zone can be explained by syn-deformation porosity generation due to creep cavitation Fusseis et al., 2009(), which is formed through coalescing originally pores at grain boundaries and triple junctions due to local dilatancy during grain boundary sliding Menegon et al., 2015(). The grain boundary sliding may close one cavity but open another pore nearby, thus

producing a grain-scale pressure differences between two neighboring pores Fusseis et al., 2009Menegon et al., 2015(;). Both field and laboratory observations of ductile shear zones found the fluid concentrates at areas of reduced grain size Precigout et al., 2017Precigout et al., 2019(;), which causes a significant drop in strength of a fault. The opening of new pores is accompanied with second-phase precipitations Precigout et al., 2017(), which inhibits the grain growth, thereby maintaining the strain localization Menzies et al., 2014(). Even if the fluid had diffused for the time range of more than 1000 Myr and the fluid migration rate is higher than the estimation of 10 m Myr^{-1} Connolly and Podladchikov, 2004(), the maintained grain size reduction may still yield a weaker zone than surroundings. In this case, the conductor C4 in the lower crust and topmost mantle is likely to be related to the interconnected magnetite formed during serpentinization. Such microphysical processes explain how the fluid and deformation process control current strain localizations in those faults of high D_{max}. The conductor C4 is directly linked to C3 and C2, which might have enhanced the activity of the faults f10 and f290. The mantle conductor C4 is horizontally connected to another major shallow-mantle conductor at CDP 20000-22000, which appears to be connected to the conductor C1 to the east. C1 might have affect the activity of f82 and f688.

Compared with those active faults cut by the high-conductivity patches in the MT profile, faults not directly cutting those conductors (f50, f29 or f02) also have relatively high displacement. The dip angle for f50, f29 and f02 are measured to be ~30^{o}. According to the Anderson faulting theory Anderson, 1905(), these faults are at a preferred reactivation angle for reverse faults. Those faults cutting high-conductivity zones with slightly higher dip angles (~45^{o}) can be reactivated with lower frictional strength than faults with lower dip angles Sibson, 1995(). The lower frictional strength may be attributed to the fluids that are indicated by the high-conductivity anomalies. Our hypothesis of fluid-assisted faulting beneath the Nullarbor Plain is consistent with previous hypotheses for lower crustal fluid-assisted faulting in the adjacent Flinders Ranges paleo-rift system Balfour et al., 2015() and possible role of mantle-derived fluids in neotectonic faulting within the Great Artesian Basin Keppel et al., 2020Ring et al., 2016(;) in southern and central parts of Australia.

Conclusions

The 100s-meter-thick limestone overlying the Precambrian basement in the Nullarbor plain provides a unique chance to record the neotectonic faulting events in the interior of cratons. The reactivated faults or folds have accumulated 10's of meters of displacement on the surface since mid-Miocene. The neotectonic features with the largest displacements are interpreted to have the highest rates of neotectonic faulting. The fault activity in the Nullarbor Plain depends on the fault dip and fault plane frictional strength. The electrical conductivity obtained through MT observations are used to constrain fluids in the

lithosphere, which is assumed to be able to weaken a fault. The most active faults may be attributed to the inherited bedrock faults with a favored dip (~30^{o}) for reverse faults and/ or lower strength of the fault plane, which could be due to fluids either sourced from the surface or the shallow mantle.

Acknowledgement

This research was funded by the Australian Research Council through Discovery Grant #DP170103350 to M. Quigley. We acknowledge the support of Dr. Stephan Thiel and Dr. Tom Wise from the Geological Survey of South Australia providing the processed MT data. H. Yang would like to thank Prof. Brian Kennett and Prof. Hans Thybo for the discussion on the seismic reflection profiles. The petrophysical information of borehole samples from the Nullarbor Plain provided by Rapael Quentin de Gromard and his colleagues from the Geological Survey of Western Australia are also appreciated. H. Yang received the Melbourne Research Scholarship, the Baragwanath Travel Scholarship and the Albert Shimmins Writing-Up Award from the University of Melbourne to assist in research development.

Open Research

All the geophysical data are downloaded from the dataset archived by Geoscience Australia. The total magnetic intensity and Bouguer Gravity data of Australia are available through https://portal.ga.gov.au/persona/gads. The seismic reflection profiles are obtained from https://data.gov.au/dataset/ds-ga-f1a18818-7700-6191-e044-00144fdd4fa6/details?q= and http://dx.doi.org/10.11636/Record.2019.006. The MT surveys used in this study are from http://pid.geoscience.gov.au/dataset/ga/122188. The fault displacement data have been uploaded to the supplementary material as a table for peer review and eventually will be uploaded to Mendeley for public access.

References

Anderson, E., 1905, The dynamics of faulting: Transactions of the Edinburgh Geological Society, v. 8, no. 3, p. 387-402.Artemieva, I. M., 2006, Global 1× 1 thermal model TC1 for the continental lithosphere: implications for lithosphere secular evolution: Tectonophysics, v. 416, no. 1-4, p. 245-277.Artemieva, I. M., and Mooney, W. D., 2001, Thermal thickness and evolution of Precambrian lithosphere: A global study: Journal of Geophysical Research-Solid Earth, v. 106, no. B8, p. 16387-16414.Balfour, N. J., Cummins, P. R., Pilia, S., and Love, D., 2015, Localization of intraplate deformation through fluid-assisted faulting in the lower-crust: The Flinders Ranges, South Australia: Tectonophysics, v. 655, p. 97-106.Becken, M., and Ritter, O., 2012, Magnetotelluric

studies at the San Andreas Fault Zone: implications for the role of fluids: Surveys in Geophysics, v. 33, no. 1, p. 65-105.Bezada, M. J., and Smale, J., 2019, Lateral variations in lithospheric mantle structure control the location of intracontinental seismicity in Australia: Geophysical Research Letters, v. 46, no. 22, p. 12862-12869.Brace, W. F., and Kohlstedt, D. L., 1980, Limits on Lithospheric Stress Imposed by Laboratory Experiments: Journal of Geophysical Research, v. 85, no. Nb11, p. 6248-6252.Burnett, S., Webb, J. A., White, S., Lipar, M., Ferk, M., Barham, M., O'Leary, M. J., and Glover, F. S., 2020, Etched linear dunefields of the Nullarbor Plain; A record of Pliocene-Pleistocene wind patterns across southern Australia: Palaeogeography, Palaeoclimatology, Palaeoecology, v. 557, p. 109911.Clark, D., McPherson, A., and Van Dissen, R., 2012, Long-term behaviour of Australian stable continental region (SCR) faults: Tectonophysics, v. 566, p. 1-30.Coblentz, D. D., Sandiford, M., Richardson, R. M., Zhou, S. H., and Hillis, R., 1995, The Origins of the Intraplate Stress-Field in Continental Australia: Earth and Planetary Science Letters, v. 133, no. 3-4, p. 299-309.Connolly, J. A. D., and Podladchikov, Y. Y., 2004, Fluid flow in compressive tectonic settings: Implications for midcrustal seismic reflectors and downward fluid migration: Journal of Geophysical Research: Solid Earth, v. 109, no. B4.Constable, S., 1993, Conduction by Mantle Hydrogen: Nature, v. 362, no. 6422, p. 704-704.Costelloe, R. D., Fomin, T., and Holzschuh, J., 2012, L201 Albany Fraser Orogen Deep Crustal Reflection Seismic Survey, WA. Stacked and migrated seismic data and images for lines AF1, AF2, AF3 and T1, Geoscience Australia, Canberra.Cowie, P. A., and Scholz, C. H., 1992a, Growth of Faults by Accumulation of Seismic Slip: Journal of Geophysical Research-Solid Earth, v. 97, no. B7, p. 11085-11095.-, 1992b, Physical Explanation for the Displacement Length Relationship of Faults Using a Post-Yield Fracture-Mechanics Model: Journal of Structural Geology, v. 14, no. 10, p. 1133-1148.Ellis, S., Van Dissen, R., Eberhart-Phillips, D., Reyners, M., Dolan, J. F., and Nicol, A., 2017, Detecting hazardous New Zealand faults at depth using seismic velocity gradients: Earth and Planetary Science Letters, v. 463, p. 333-343.Fagereng, Å., and Biggs, J., 2019, New perspectives on 'geological strain rates' calculated from both naturally deformed and actively deforming rocks: Journal of Structural Geology, v. 125, p. 100-110.Fusseis, F., Regenauer-Lieb, K., Liu, J., Hough, R. M., and De Carlo, F., 2009, Creep cavitation can establish a dynamic granular fluid pump in ductile shear zones: Nature, v. 459, no. 7249, p. 974-977.Glover, P. W. J., 1996, Graphite and electrical conductivity in the lower continental crust: a review: Physics and Chemistry of the Earth, v. 21, no. 4, p. 279-287.Holzschuh, J., 2015, 13GA–EG1 Eucla-Gawler Seismic Survey–Acquisition and Processing of the western Gawler Craton section, Geoscience Australia, Canberra.Hou, B., Frakes, L. A., Sandiford, M., Worrall, L., Keeling, J., and Alley, N. F., 2008, Cenozoic Eucla Basin and associated palaeovalleys, southern Australia—climatic and tectonic influences on landscape evolution, sedimentation and heavy mineral accumulation: Sedimentary Geology, v. 203, no. 1-2, p. 112-130.Johnston, A. C., 1989, The seismicity of 'stable continental interiors', Earthquakes at North-Atlantic passive margins: Neotectonics and postglacial rebound, Springer, p. 299-327.Kagan, Y. Y., 1997, Seismic mo-

ment-frequency relation for shallow earthquakes: Regional comparison: Journal of Geophysical Research: Solid Earth, v. 102, no. B2, p. 2835-2852.Karato, S., and Jung, H., 1998, Water, partial melting and the origin of the seismic low velocity and high attenuation zone in the upper mantle: Earth and Planetary Science Letters, v. 157, no. 3-4, p. 193-207.Keppel, M. N., Karlstrom, K. E., Crossey, L., Love, A. J., and Priestley, S., 2020, Evidence for intra-plate seismicity from spring-carbonate mound springs in the Kati Thanda–Lake Eyre region, South Australia: implications for groundwater discharge from the Great Artesian Basin: Hydrogeology Journal, v. 28, no. 1, p. 297-311.King, T. R., Quigley, M., and Clark, D., 2019, Surface-Rupturing Historical Earthquakes in Australia and Their Environmental Effects: New Insights from Re-Analyses of Observational Data: Geosciences, v. 9, no. 10, p. 408.Kirkland, C. L., Smithies, R. H., Spaggiari, C. V., Wingate, M. T. D., De Gromard, R. Q., Clark, C., Gardiner, N. J., and Belousova, E. A., 2017, Proterozoic crustal evolution of the Eucla basement, Australia: Implications for destruction of oceanic crust during emergence of Nuna: Lithos, v. 278, p. 427-444.Lenardic, A., Moresi, L. N., and Mühlhaus, H., 2003, Longevity and stability of cratonic lithosphere: Insights from numerical simulations of coupled mantle convection and continental tectonics: Journal of Geophysical Research: Solid Earth, v. 108, no. B6, p. n/a-n/a.Leonard, M., Burbidge, D., Allen, T., Robinson, D., McPherson, A., Clark, D., and Collins, C., 2014, The challenges of probabilistic seismic-hazard assessment in stable continental interiors: An Australian example: Bulletin of the Seismological Society of America, v. 104, no. 6, p. 3008-3028.Lockner, D. A., Morrow, C., Moore, D., and Hickman, S., 2011, Low strength of deep San Andreas fault gouge from SAFOD core: Nature, v. 472, no. 7341, p. 82-85.Lowry, D. C., and Jennings, J. N., 1974, The Nullarbor karst Australia: Zeitschrift für Geomorphologie, v. 18, no. 1, p. 35-81.Mansfield, C., and Cartwright, J., 2001, Fault growth by linkage: observations and implications from analogue models: Journal of Structural Geology, v. 23, no. 5, p. 745-763.Menegon, L., Fusseis, F., Stunitz, H., and Xiao, X. H., 2015, Creep cavitation bands control porosity and fluid flow in lower crustal shear zones: Geology, v. 43, no. 3, p. 227-230.Menzies, C. D., Teagle, D. A. H., Craw, D., Cox, S. C., Boyce, A. J., Barrie, C. D., and Roberts, S., 2014, Incursion of meteoric waters into the ductile regime in an active orogen: Earth and Planetary Science Letters, v. 399, p. 1-13.Miller, C. R., James, N. P., and Bone, Y., 2012, Prolonged carbonate diagenesis under an evolving late cenozoic climate; Nullarbor Plain, southern Australia: Sedimentary Geology, v. 261, p. 33-49.Naliboff, J., and Buiter, S. J. H., 2015, Rift reactivation and migration during multiphase extension: Earth and Planetary Science Letters, v. 421, p. 58-67.Precigout, J., Prigent, C., Palasse, L., and Pochon, A., 2017, Water pumping in mantle shear zones: Nature Communications, v. 8, no. 1, p. 1-10.Precigout, J., Stunitz, H., and Villeneuve, J., 2019, Excess water storage induced by viscous strain localization during high-pressure shear experiment: Scientific Reports, v. 9, no. 1, p. 1-9.Quigley, M. C., Clark, D., and Sandiford, M., 2010, Tectonic geomorphology of Australia: Australian Landscapes, v. 346, no. 1, p. 243-265.Raimondo, T., Clark, C., Hand, M., Cliff, J., and Anczkiewicz, R., 2013, A simple mechanism for mid-crustal shear zones to record surface-derived

fluid signatures: Geology, v. 41, no. 6, p. 711-714.Rajabi, M., Tingay, M., Heidbach, O., Hillis, R., and Reynolds, S., 2017, The present- day stress field of Australia: Earth-Science Reviews, v. 168, p. 165-189.Ring, U., Uysal, I. T., Yuce, G., Unal-Imer, E., Italiano, F., Imer, A., and Zhao, J. X., 2016, Recent mantle degassing recorded by carbonic spring deposits along sinistral strike-slip faults, south-central Australia: Earth and Planetary Science Letters, v. 454, p. 304-318.Robertson, K., Taylor, D., Thiel, S., and Heinson, G., 2015, Magnetotelluric evidence for serpentinisation in a Cambrian subduction zone beneath the Delamerian Orogen, southeast Australia: Gondwana Research, v. 28, no. 2, p. 601-611.Sandiford, M., and Quigley, M., 2009, TOPO-OZ: Insights into the various modes of intraplate deformation in the Australian continent: Tectonophysics, v. 474, no. 1-2, p. 405-416.Sandiford, M., Wallace, M., and Coblentz, D., 2004, Origin of the in situ stress field in south-eastern Australia: Basin Research, v. 16, no. 3, p. 325-338.Scheib, A., Morris, P., Murdie, R., and Delle Piane, C., 2016, A passive seismic approach to estimating the thickness of sedimentary cover on the Nullarbor Plain, Western Australia: Australian Journal of Earth Sciences, v. 63, no. 5, p. 583-598.Sibson, R. H., 1995, Selective fault reactivation during basin inversion: potential for fluid redistribution through fault-valve action: Geological Society, London, Special Publications, v. 88, no. 1, p. 3-19.Stesky, R. M., and Brace, W. F., 1973, Electrical Conductivity of Serpentinized Rocks to 6 Kilobars: Journal of Geophysical Research, v. 78, no. 32, p. 7614-7621.Thiel, S., and Heinson, G., 2010, Crustal imaging of a mobile belt using magnetotellurics: An example of the Fowler Domain in South Australia: Journal of Geophysical Research-Solid Earth, v. 115, no. B6.Walsh, J. J., Nicol, A., and Childs, C., 2002, An alternative model for the growth of faults: Journal of Structural Geology, v. 24, no. 11, p. 1669-1675.Wells, D. L., and Coppersmith, K. J., 1994, New Empirical Relationships among Magnitude, Rupture Length, Rupture Width, Rupture Area, and Surface Displacement: Bulletin of the Seismological Society of America, v. 84, no. 4, p. 974-1002.Wise, T., Pawley, M., Thiel, S., and Dutch, R., 2018, Geology, geophysics, geochemistry of a hidden Palaeoproterozoic ocean-continent transition in the northern Gawler Craton: ASEG Extended Abstracts, v. 2018, no. 1, p. 1-5.Wise, T., and Thiel, S., 2019, Proterozoic tectonothermal processes imaged with magnetotellurics and seismic reflection in southern Australia: Geoscience Frontiers.Xu, Y., Shankland, T. J., and Poe, B. T., 2000, Laboratory-based electrical conductivity in the Earth's mantle: Journal of Geophysical Research: Solid Earth, v. 105, no. B12, p. 27865-27875.Yang, H., Chemia, Z., Artemieva, I. M., and Thybo, H., 2018, Control on off-rift magmatism: A case study of the Baikal Rift Zone: Earth and Planetary Science Letters, v. 482, p. 501-509.Yang, H., Quigley, M., and King, T. R., 2021, Surface slip distributions and geometric complexity of intraplate reverse-faulting earthquakes: GSA Bulletin.

Figures

Figure 1. (**a**) Topographic map of the Nullarbor Plain, Australia. Black (or red) lines mark the mapped neotectonic fold (or fault) traces on the surface. The circles are regional earthquakes (1970-2020) from the Geoscience Australia catalog. The traces in the northwestern part are demarcated by a shaded polygon, which is referred to as the interior region in this study. The dashed yellow contours represent annual precipitations. The inset map illustrates tectonic settings of the study area, which is located between the Archean Yilgarn and Gawler craton. Displacement for each trace is measured. The maximum and average displacement versus fault length is shown in (**b**) and (**c**), respectively. The light grey dots represent data from the Northwestern part, shaded polygon in (**a**). Some of these traces that have a relatively high displacement or length are labeled with the number of each trace, which is shown in (**a**) adjacent to each fault trace. The label colors in (**b**) and (**c**) are also consistent with the fault color in (**a**). The red one generally has high displacements.

Figure 2. (**a**) Tectonic settings in the Nullarbor plain shown on the total magnetic intensity map (https://portal.ga.gov.au/persona/gads). (**b**) Migrated seismic reflection profiles, 12GA-AF3 and 13GA-EG1, crossing the Nullarbor Plain. The vertical axis of the seismic profile is the two-way time (TWT, 0-20 s), and the time-to-depth conversion is calculated with the velocity of 6 km s^{-1}.

Figure 3. (**a**) Tectonic settings in the Nullarbor plain shown on the Bouguer Gravity anomaly map (https://portal.ga.gov.au/persona/gads). (**b**) MT profiles co-located with the 12GA-AF3 and 13GA-EG1 seismic reflection profiles crossing the Nullarbor plain. The MT profile is divided into two parts, due to the NNE striking structures to the east and the predominant N-S oriented strike to the west. The white dashed line is at the depth of 25 km, which is used to delimit the lower boundary for most of the upper crustal conductors and the upper boundary for the lower crustal conductors.

Figure 4. Interpretation of the overlapped seismic and MT profiles. For the surface-mapped faults that have corresponding reflectors on the seismic profile, those with a relatively high D_{max} and adjacent to the electrical conductors are coded with red color, otherwise, they are illustrated by black lines. The fault f290 is not directly cut by the profile, but assumed to be if northward extended, so it is marked with red dashed line. Red color in the MT profile denotes high conductivity and blue low conductivity.